Spectra stitching for ultra-high resolution, low sensitivity decay and high-speed SD-OCT

Maria, Michael; Anisimov, Andrei G.; Stols-Witlox, Maartje; Groves, Roger M.

DOI
10.1117/12.2545157

Publication date
2020

Document Version
Final published version

Published in
Design and Quality for Biomedical Technologies XIII

Spectra stitching for ultra-high resolution, low sensitivity decay and high-speed SD-OCT

Maria, Michael, Anisimov, Andrei, Stols-Witlox, Maartje, Groves, Roger

Michael Maria, Andrei G. Anisimov, Maartje Stols-Witlox, Roger M. Groves, "Spectra stitching for ultra-high resolution, low sensitivity decay and high-speed SD-OCT," Proc. SPIE 11231, Design and Quality for Biomedical Technologies XIII, 1123104 (17 February 2020); doi: 10.1117/12.2545157

SPIE.

Event: SPIE BiOS, 2020, San Francisco, California, United States

Spectra stitching for ultra-high resolution, low sensitivity decay and high-speed SD-OCT

Michael Maria*[a], Andrei G. Anisimov[a], Maartje Stols-Witlox[b] and Roger M. Groves[a]
[a]Structural Integrity and Composites, Faculty of Aerospace Engineering, Delft University of Technology, Kluyverweg 1, 2629 HS Delft, The Netherlands
[b]Conservation & Restoration, University of Amsterdam, Johannes Vermeerplein 1, 1071 DV Amsterdam, The Netherlands

ABSTRACT

In this study we investigate the possibility of spectra stitching in the context of Spectral Domain – Optical Coherence Tomography (SD-OCT). The aim is to reach a high axial resolution while keeping sampling issues to a low level (slow decay in depth) but still operating with the fastest camera line rate available. The paper focuses mainly on simulations of spectrometer signals and the stitching procedure. It briefly introduces the experimental system. The findings of this study are relevant to most of the SD-OCT systems and could also be transferred to Swept Source OCT (SS-OCT) where they will help to increase the axial resolution capabilities.

Keywords: *Optical Coherence Tomography, Spectrometer, Imaging, Optical Noise, Spectra Stitching*

1. INTRODUCTION

Fourier-Domain Optical Coherence Tomography (FD-OCT) is an imaging modality based on low coherence interferometry that can be used for accurate reconstruction of 3D images of scattering samples [1]. The OCT technology can be split into two main sub-groups: Swept-source OCT (SS-OCT) and Spectral-Domain OCT (SD-OCT). In SS-OCT, the system consists of a fast-tunable laser, an interferometer and a fast photo-diode acting as the detector. In this situation the detected signal is sampled in time and a time-to-frequency mapping is used to infer the spectral distribution. In SD-OCT, the system consists of a broad light source, an interferometer and a spectrometer. In this case, the signal is directly sampled in wavelength domain using a diffraction element such as a diffraction grating. In both cases, the acquired interference signal is a discrete representation of the light intensity as a function of wavelength. This signal is a sum of a direct current term and an interference term. Optical Coherence Tomography technology relies on frequency analysis of the interference signal to locate reflective centers within the sample of interest. Considering the case of SD-OCT, with a spectrometer used as a sampling device, a complex situation arises as high sensitivity, large imaging depth and high speed can only be reached when different parameters are optimized [2]. The difficulty lies in the opposite influence of some parameters such as the number of pixels or the spectral range of the spectrometer. For example, an SD-OCT requires a large optical bandwidth for high resolution imaging, as a results the spectrometer spectral resolution tends to become relatively large. High spectral resolution leads to high sensitivity decay and a shorter imaging range for the system. These types of conflicts affect the optimization of the system: imaging speed versus number of pixels, number of pixels versus geometrical aberrations, etc. Figure 1 shows a sketch that summarizes the several possible interactions of the spectrometer parameters on the SD-OCT metrics.

Numerous studies have been conducted in order to reduce the impact of some parameters involved in spectrometer design. Depending on the application of the OCT system, compromises are sometimes possible that favor one parameter over another. If speed is not a main concern, increasing the number of pixels in the camera to above 8192 pixels drastically reduces the sampling issue [3, 4] for optical bandwidths in the hundreds nm range. However, such a design increases the problem of optical aberrations by using a longer pixel line. Another solution for reducing spectral sampling issues and sensitivity decay is to use a linear-in-angular-wavenumber spectrometer. Rolland & al. recently demonstrated the power of freeform optics in that context [5]. Nonetheless, this comes with more complicated spectrometer design that often leads to a not ultra-broad spectral range. Contra, if speed is a key parameter (i.e. for eye examination), the number of pixels cannot be increased as it leads to significant speed limitations. Then, a spectrometer design with high density grating lines and custom design optics has shown relatively low sensitivity decay (<10 dB/mm) [6,7]. Finally, a change in the central wavelength can eventually lead to a higher axial resolution with lower spectral bandwidth, yet such a solution cannot be applied to any sample. Indeed, a different central wavelength can be used only if the sample of interest shows enough

Design and Quality for Biomedical Technologies XIII, edited by Jeeseong Hwang, Gracie Vargas, Proc. of SPIE
Vol. 11231, 1123104 · © 2020 SPIE · CCC code: 1605-7422/20/$21 · doi: 10.1117/12.2545157

transparency over a large spectral band. For example, using visible light for skin imaging instead of the more common 1300 nm band [8,9], leads to very shallow imaging due to high scattering of visible light by skin.

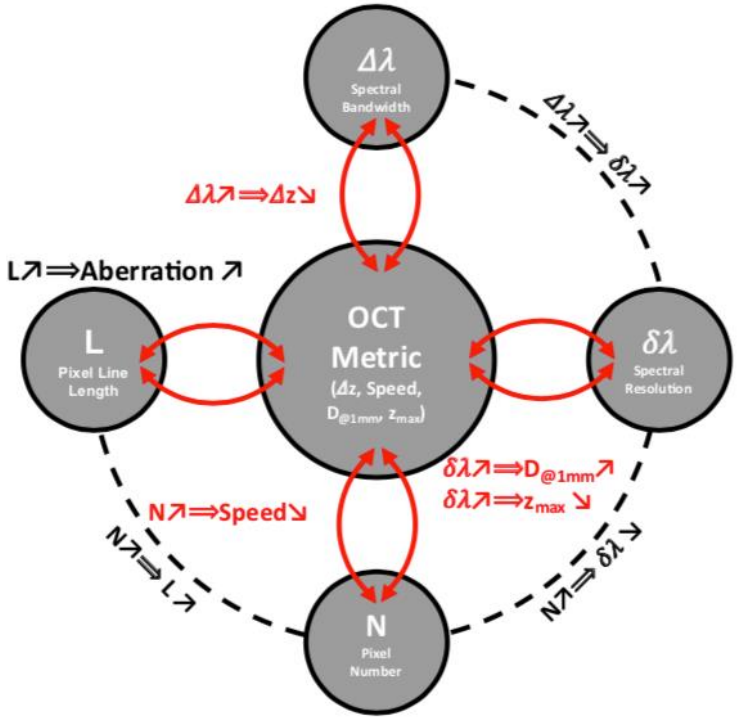

Figure 1: Conceptual sketch describing the influence of spectrometer parameters on OCT system specifications. Δz is the axial resolution, $D_{@1mm}$ is the sensitivity decay at 1 mm axial position and z_{max} is the maximum axial position of the OCT system.

In this study we present a novel approach to reduce the constraints on spectrometer design when aiming for high resolution, low sensitivity decay and high-speed SD-OCT. Our approach relies on using two separated spectrometers with overlapping spectra to detect the interference signal and stitching the resulting spectra prior to a Fast Fourier Transform (FFT) operation. Doing so, the number of pixels is effectively increased and hence a finer spectral resolution (improved imaging range and low sensitivity decay) is obtained while working with an ultra-broad spectral range (300 nm). However, thanks to the two cameras, a low level of geometrical aberrations and a high readout speed are maintained comparable to the level of a spectrometer with a lower pixel number. The results presented here contribute towards closing the gap between high speed SD-OCT and ultra-high-resolution SD-OCT. In this paper, we introduce the results obtained in the modelling of the stitching procedure, in which the spectra stitching approach consists of a direct point-based stitching of two spectra within an overlapping region.

2. STITCHING PROCEDURE MODELLING

2.1 Context of the study

The current report describes preliminary results obtained by investigating spectra stitching from multiple cameras within an SD-OCT configuration. In that context, three spectrometers have to be considered, 2 real and 1 virtual. The two real spectrometers are the ones used to record the interference signals at the output of the interferometer (prior to stitching). The virtual spectrometer is the one the stitching procedure aims to obtain. In the following sections, in order to clearly distinguish between the spectrometer, Spectrometer "1" is called "Blue/Green (BG)", Spectrometer "2" is called "Yellow/Red (YR)" and Spectrometer "3" is called Blue/Red (BR)". The main parameters of the three spectrometers are described below in Table 1. Also, within the next sections, two spectral shapes are considered. They represent the readouts from the two real spectrometers (BG & YR) if illuminated with light sources with Gaussian power spectral densities with respective central wavelengths of 475 nm and 600 nm and Full-Width-Half-Maximum (FWHM) bandwidths of 50 nm.

Table 1: Specifications of the three spectrometers (2 real and 1 virtual) considered in the spectra stitching study.

	Spectrometer BG (real)	Spectrometer YR (real)	Spectrometer BR (virtual)
Start Wavelength [nm]	400	500	400
Stop Wavelength [nm]	550	700	700
Start Angular Wavenumber [rad.nm^{-1}]	0.0157	0.0126	0.0157
Stop Angular Wavenumber [rad.nm^{-1}]	0.0114	0.0090	0.0090
Spectral Resolution [nm]	0.0732	0.0977	0.0732
Spectral Resolution [rad.nm^{-1}]	2.10 x 10^{-6}	1.76 x 10^{-6}	1.63 x 10^{-6}
Pixel Number [cts]	2048	2048	4096

2.2 Calibration for spectra stitching

Commonly, SD-OCT requires a processing step called resampling [10]. Data generated at the output of a spectrometer is a discrete representation of the light intensity as a function of the pixel position. The pixel line distribution can be mapped into a non-linear distribution of wavelengths and hence a non-linear distribution of angular wavenumbers $k = 2\pi/\lambda$. As angular wavenumber and optical path difference are conjugate variables through FFT operation, it is necessary to perform an interpolation of the interference signal data points in order to obtain a discrete signal along a linear-in-angular-wavenumber x-axis (see Fig. 2).

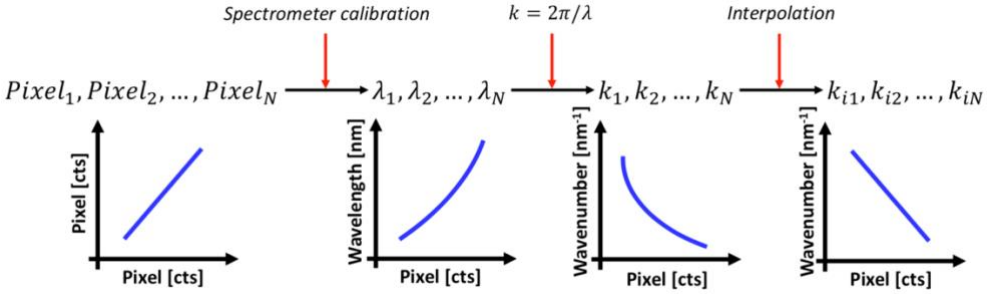

Figure 2: Representation of the step-by-step procedure required to obtain a linear-in-angular-wavenumber distribution for the angular wavenumber axis prior to FFT operation.

When considering the spectra stitching context, an additional parameter comes into play regarding the resampling step. The aim of the stitching procedure is to reduce some design constraints (finite pixel readout speed, geometrical aberrations, etc.) of the spectrometer by using two distinct spectrometers. Nevertheless, the core of the SD-OCT analysis still remains, meaning that an FFT operation is still required to relate an axial profile to the interference signal. Hence, the stitched spectrum needs to be interpolated as described by Fig. 2. The difference bring by the stitching step, compared with the common resampling procedure used in SD-OCT, is that the two spectra from the real spectrometers need to be resampled by considering the spectral properties of the third (virtual) spectrometer.

Figure 3(a) shows spectral shape of the Spectrometer Blue/Red consisting of a discrete signal of length 4096 pixels distributed equally along the angular wavenumber axis covering from 0.009 rad.nm^{-1} (700 nm) and 0.0157 rad.nm^{-1} (400

nm). The spectra stitching adapted resampling procedure interpolates the real spectra (Blue/Green and Yellow/Red) within the same wavelength axis (black lines) instead of the single spectrometer axis (blue and red lines). While it is expected that the spectral shapes after interpolation do not change, one noticeable effect is that the length of the two interpolated spectra from the real spectrometers, increases. This is due to the fact that the spectral resolution of the virtual spectrometer is lower than the spectral resolutions of the two real spectrometers. The updated lengths of the two interpolated spectra are 2607 pixels for the Blue/Green spectrometer and 2185 pixels for the Yellow/Red spectrometer.

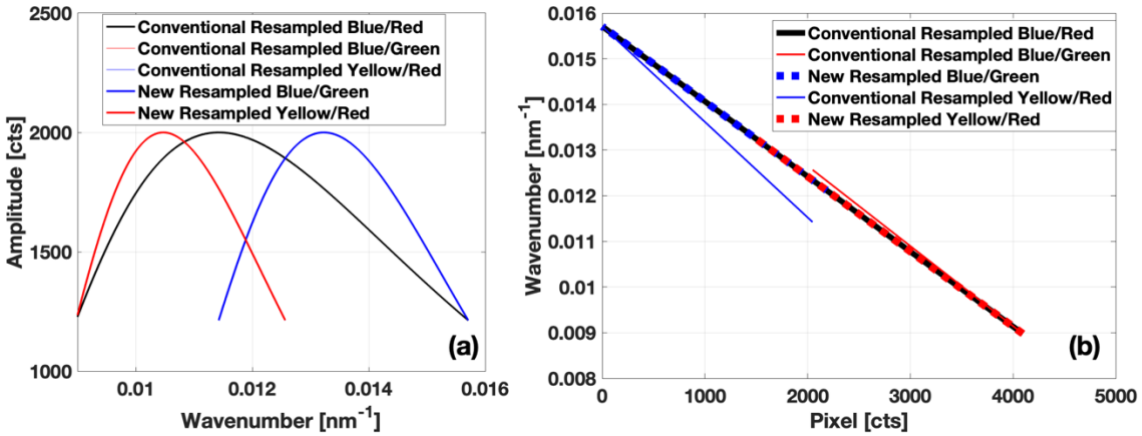

Figure 3: Illustration of the resampling of the angular wavenumber axis consideration in the context of spectra stitching (a) Spectral shapes and (b) angular wavenumber distribution along the pixel line for a conventional resampling and for the resampling considering the spectra stitching context.

2.3 Stitching spectra: Point-based stitching (noise-free)

The method used for achieving the spectra stitching relies on a point stitching approach. After interpolating the two readouts from the two real spectrometers one can select an angular wavenumber point k_{Stitch} within the overlapping region between the two spectra and create a new longer spectrum which has the new form,

$$I_{Stitched}(\lambda) = \begin{cases} I_{YR}(k) \; for \; k \in \left[k_{Start\_YR}, k_{Stitch}\right] \\ I_{BG}(k) \; for \; k \in \left[k_{Stitch}+1, k_{Stop\_BG}\right] \end{cases} \quad (1)$$

With $k_{Start\_YR} = 2\pi/\lambda_{Stop\_YR}$ and $k_{Stop\_BG} = 2\pi/\lambda_{Start\_BG}$. As the new spectrum is already properly organized with equal spacing in the angular wavenumber domain, the axial profile can be calculated using an FFT operation. Figure 4 shows the steps involved in the point stitching procedure. Figure. 4(a) shows the spectra from the two spectrometers (Fig. 4(b) is a zoom-in within the overlapping area). Figure 4(c) shows the resulting spectra after stitching. It is noticeable that the resulting spectral shape after stitching is no longer Gaussian. Such a spectral shape alters the Point Spread Function (PSF) in the frequency domain (after FFT operation). This is illustrated with Fig. 5, which is a representation in dB scale of the axial profiles obtained from the spectra represented in Fig. 4. If considered separately, the axial profiles obtained from spectrometers BG and YR (regardless of the resampling method) show almost identical shapes. The small differences which can be observed can be attributed to the modification of the spectral shapes due to the interpolation during the resampling step. In the case of the stitched spectrum (green), the PSF is distorted compared to an ideal one (with side lobes). However, this effect in amplitude space is minimal as those side lobes have a much smaller amplitude than the main peak. In the event of a strongly distorted PSF, applying a new window function would be an option to restore the PSF to its correct shape.

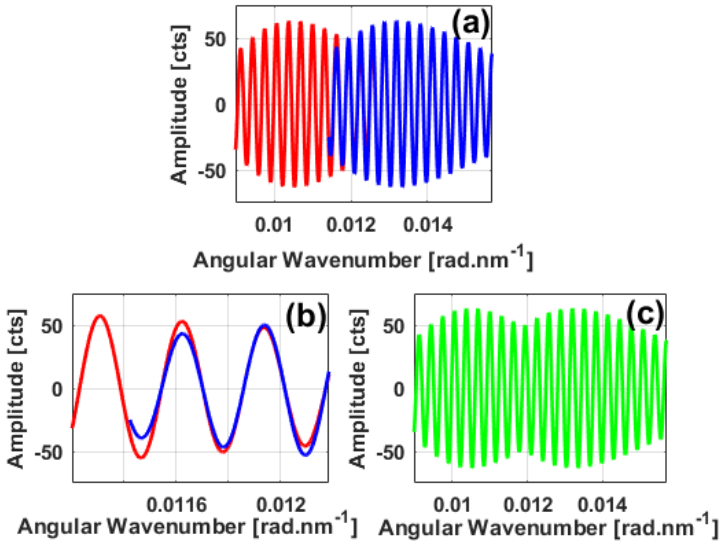

Figure 4: Simulation of the spectra stitching based on a point stitching approach – Sample: Single reflector at a depth of 100 µm. (a) Representation of two spectra from the two real spectrometers, (b) Zoom-in into the overlapping region of the two readouts, (c) Resulting spectrum after stitching at crossing point.

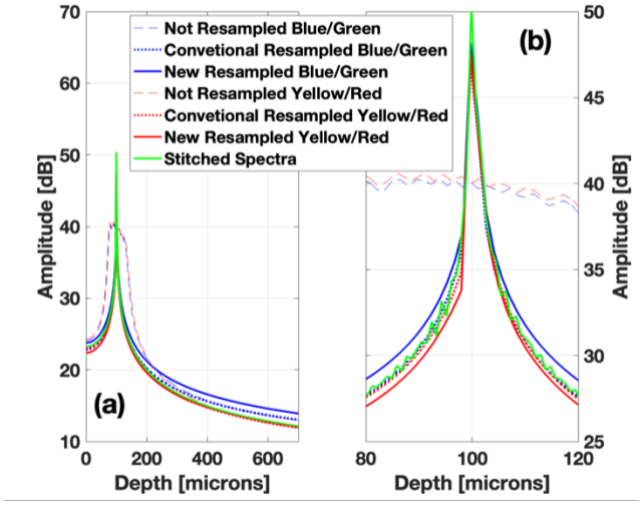

Figure 5: (a) Depth reflectivity profiles obtained from the simulated spectra of Fig.4. (b) zoom-in within the peak area of Fig. 4(a).

2.4 Stitching spectra: Importance of the phase alignment

The benefit of the spectra stitching relies on separating the detection units into two or more entities in the hardware but still processing the data as if they were acquired by a single detector. This implies, from the hardware point of view, that the light within the interferometer has to be split right before the detection. The simplest way to achieve this splitting is to use an optical beam splitter (BS). When doing so, a parameter to consider is the phase difference between the light transmitted and the light reflected by the BS (see illustration of Fig. 6). In the context of spectra stitching, this additional phase shift for the reflected light leads to spectrum which shows an anti-phase characteristic, as shown in Fig. 7(a). This new configuration is less favorable for spectra stitching as it creates a distortion point within the stitched spectrum (Fig. 7(b)). When applying an FFT operation to the stitched spectra, a poor quality PSF is generated (Fig. 7(c) and Fig. 7(d)). This PSF is characterized by strong side lobes corrupting the whole imaging range. This causes an increased noise floor and hence a lower imaging quality. It is therefore important to apply either digital or hardware-based methods to align the two spectra and to remove the anti-phase characteristic prior to stitching. This can be accomplish though both digital manipulation of one of the interference spectrum or adding extra optical components such as beam splitter or mirrors in the path of a transmitted light at the original splitting position.

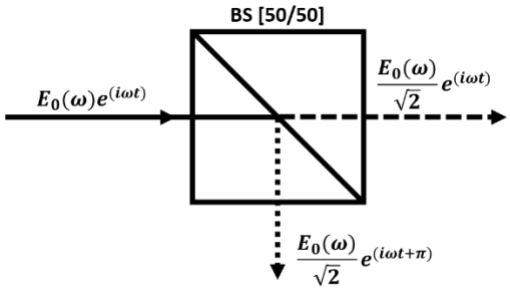

Figure 6: Illustration of the phase difference between reflected and transmitted light caused by a BS. E_0 is the light amplitude, ω is the light frequency and t is time.

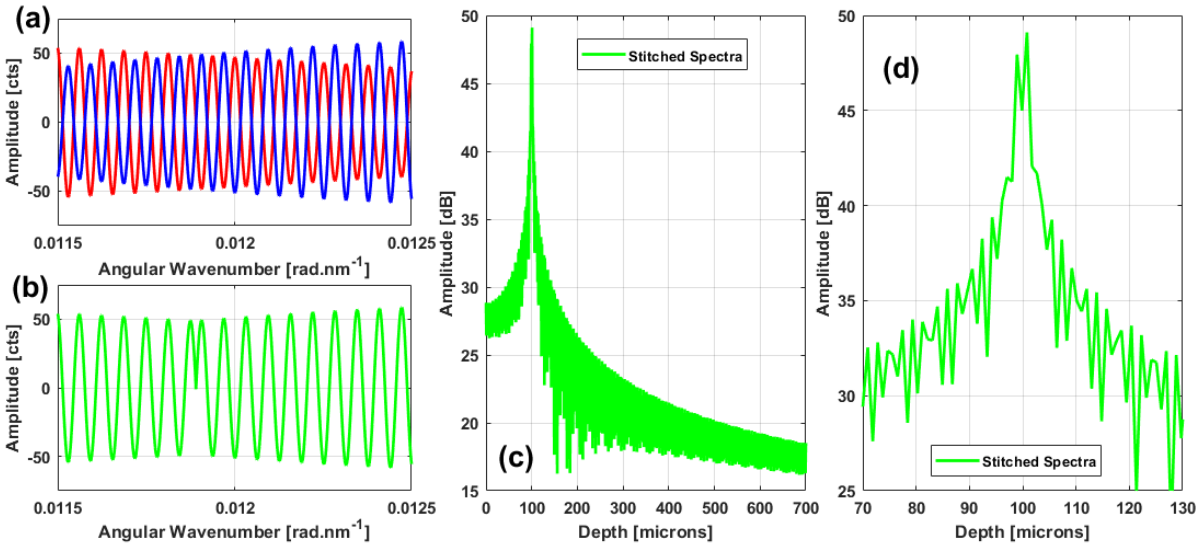

Figure 7: Illustration of phase difference impact on point-based spectra stitching. (a) Spectra with anti-phase behavior, (b) Stitched spectrum with abnormal interference fringes, (c) Axial profile of the stitched spectrum, (d) zoom-in of the peak area of Fig. 7(c).

2.5 Stitching spectra: Influence of intensity noise

An important parameter which affects any OCT system is the level of intensity noise arising in the data. Intensity noise in OCT is relatively well known and well documented [11, 12]. Three main contributions can be identified. They are electronic noise, shot noise and relative intensity noise. Briefly, the effect of intensity noise is a reduction of the signal to noise ratio of the SD-OCT system through an elevation of the noise floor within the axial profile. This is shown in Fig. 8(a) and Fig. 8(b), where the axial profile of the spectrum of Fig. 4 is plotted after considering intensity noise levels of 0% and 5% (which is the noise level reported in the literature for supercontinuum driven OCT system [11,12]) in the case of the in-phase spectra prior to stitching. The noise floor is raised by around 5 dB between the noise free case and the case with noise. In the case of the anti-phase configuration (Fig. 8(c) and Fig. 8(d)), the same noise floor elevation can be observed still with the side lobes problem mentioned above. It is important to validate the fact that intensity noise does not forbid the stitching of spectra. In real imaging conditions, intensity noise is a important part of the entire system and its effect can only be diminished and not completely cancelled.

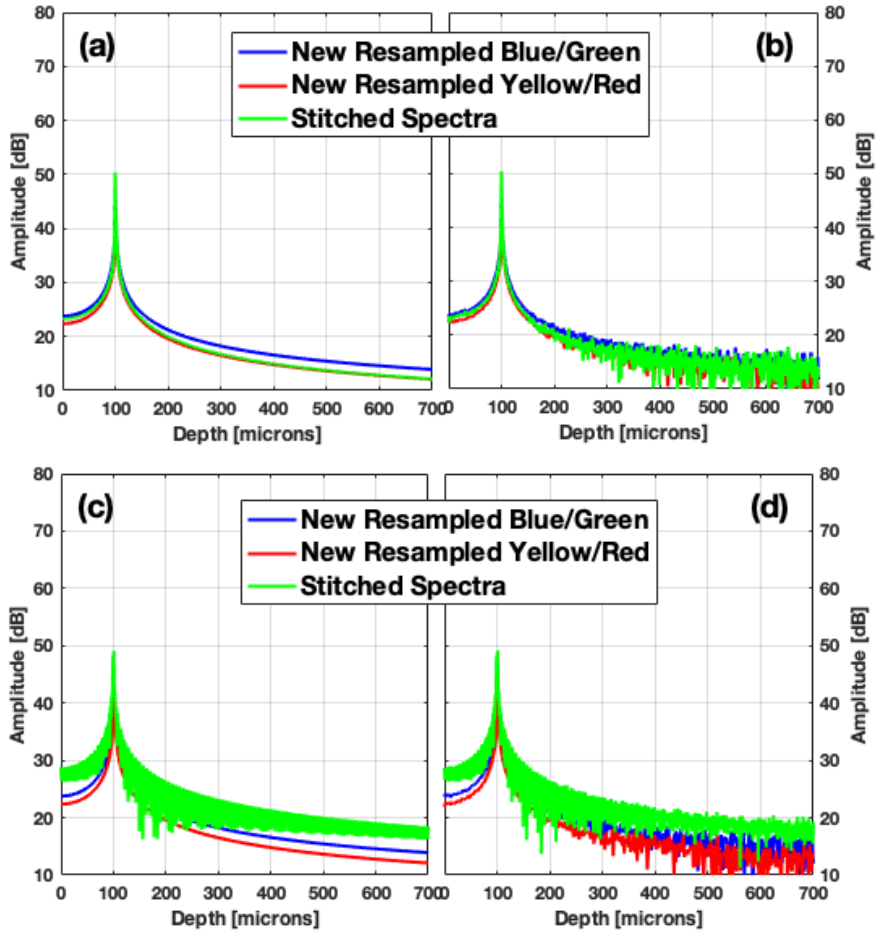

Figure 8: Axial profile modification with intensity noise. (a) noise free – in-phase spectra, (b) noise included – in-phase spectra, (c) noise free – out-of-phase spectra, (d) noise included – out-of-phase spectra.

3. EXPERIMENTAL SYSTEM DESCRIPTION

The calculation presented above was conducted in parallel with the development of a dual-spectrometer SD-OCT system. The system is based on a visible light band covering from around 450 nm (blue) up to 700 nm (red), generated and filtered from a Supercontinuum (SC) light source (Leukos ELECTRO VISIR250). The interferometer itself consists of bulk optics coated for operating in the visible range. Finally, the detection of the interference signal is obtained through two spectrometers from Wasatch Photonics (Cobra Vis). Both spectrometers use a 2048 pixels CMOS camera (E2V OctoPlus). The first spectrometer (BR) covers a spectral range from 400 nm to 550 nm and the second spectrometer (TR) covers a spectral range from 500 nm to 700 nm. The 50 nm overlap is used to optimize the stitching procedure. The two spectrometers are connected to the bulk-based interferometer using a pair of optical fibers and parabolic reflectors. Figure 2 is a top-view of a 3D representation of the system. Figure 10 is an example of the spectral shapes detected at the output of the interferometer. It is noticeable that the two shapes differ greatly from the Gaussian ones used during the modelling. Additional pre-processing is necessary to adapt the two spectra and thus avoid distortion cause by amplitude mismatch and will be the topic of the next phase of the research.

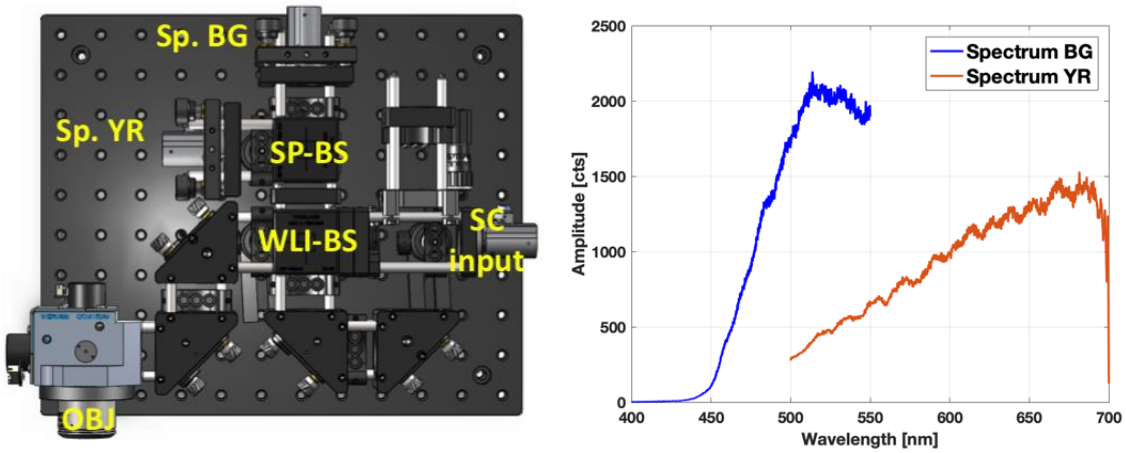

Figure 9: Top-view of a 3D drawing of the bulk interferometer and the spectral shapes detected by spectrometer BG and spectrometer YR. Sp.BG is the Blue/Green spectrometer input, Sp.YR is the Yellow/Red spectrometer input, SP-BS is the Spectra splitting beam splitter, WLI-S is the White Light Interferometer Beam Splitter, SC input is the Supercontinuum light input and OBJ is the Objectif focusing light onto the sample.

4. CONCLUSION

To conclude, this paper shares the preliminary results of a new approach that aims on increasing the pixel number in OCT readouts by using separate cameras, covering spectral ranges with a small overlap. A model describing the influence of the phase difference between the two stitched spectra showed that particular care needs to be taken to prevent distorted spectral shape of the PSF in the Fourier domain. Indeed, important distortions of the PSF occur due to perturbation of the interference fringes. Proper phase alignment between the signals detected by each spectrometer leads to a great reduction of the side lobes issue. Also, the intensity noise influence is briefly discussed, as it needs to be dealt with in order to ensure that amplitude mismatch caused by optical noise does not create an additional issue for the stitching algorithm.

5. ACKNOWLEDGMENT

This work is supported by the Dutch Research Council (NWO) through the project Down To The Ground (VC.GW17.029).

REFERENCES

[1] Huang, D., Swanson, E. A., Lin, C.P., Schuman, J. S., Stinson, W. G., Chang, W., Hee, M. R., Flotte, T., Gregory, K., Puliafito, C. A., Fujimoto, J. G., "Optical Coherence Tomography," Science 254(5035), 1178-1181 (1991).

[2] Uribe-Patarroyo, N., Kassani, S. H., Villiger, M., and Bouma, B.E., "Robust wavenumber and dispersion calibration for Fourier-domain optical coherence tomography," Opt. Express 26(7), 9081-9094 (2018).

[3] Harper, D. J., Augustin, M., Lichtenegger, A., Eugui, P., Reyes, C., Glösmann, M., Hitzenberger, C. K. and Baumann, B. "White light polarization sensitive optical coherence tomography for sub-micron axial resolution and spectroscopic contrast in the murine retina," Biomed. Opt. Express 9, 2115-2129 (2018).

[4] Lichtenegger, A., Harper, D. J., Augustin, M., Eugui, P., Muck, M., Gesperger, J., Hitzenberger, C. K., Woehrer, A. and Baumann, B. "Spectroscopic imaging with spectral domain visible light optical coherence microscopy in Alzheimer's disease brain samples," Biomed. Opt. Express 8(9), 4007-4025 (2017).

[5] Yoon, C., Bauer, A., Xu, D., Dorrer, C. and Rolland, J. P. "Absolute linear-in-k spectrometer designs enabled by freeform optics," Opt. Express 27(24), 34593-34602 (2019).

[6] Unknown, "Cobra OCT Spectrometers," Wasatch Photonics, 08 January 2020, https://wasatchphotonics.com/product-category/optical-coherence-tomography/cobra-oct-spectrometers/ (08 January 2020).

[7] Unknown, "Compact OCT Optical Spectrometer", Gooch & Housego, 01 June 2018, https://gandh.com/wp-content/uploads/2016/01/GH-DS-FO-assemblies-compact-oct-optical-spectrometer.pdf (08 January 2018).

[8] Israelsen, N. M., Maria, M., Mogensen, M., Bojesen, S., Jensen, M., Haedersdal, M., Podoleanu, A., and Bang, O. "The value of ultrahigh resolution OCT in dermatology - delineating the dermo-epidermal junction, capillaries in the dermal papillae and vellus hairs," Biomed. Opt. Express 9(5), 2240-2265 (2018).
[9] Mogensen, M., Bojensen, S., Israelsen, N. M., Maria, M., Jensen, M., Podoleanu, A., Bang, O. and Haedersdal, M., "Two optical coherence tomography systems detect topical gold nanoshells in hair follicles, sweat ducts and measure epidermis," J. Biophotonics. 2018; 11:e201700348. https://doi.org/10.1002/jbio.201700348
[10] Bradu, A., Israelsen, N.M., Maria, M., Marques, M. J., Rivet, S., Feuchter, T., Bang, O. and Podoleanu, P. Recovering distance information in spectral domain interferometry. Sci Rep 8, 15445 (2018) doi:10.1038/s41598-018-33821-0
[11] Jensen, M., Gonzalo, I. B., Engelsholm, R. D., Maria, M., Israelsen, N. M., Podoleanu and A. Bang, O. "Noise of supercontinuum sources in spectral domain optical coherence tomography," J. Opt. Soc. Am. B 36, A154-A160 (2019).
[12] Maria, M., Gonzalo, I. B., Bondu, M., Engelsholm, R. D., Feuchter, T., Moselund, P.M., Leick, L., Bang, O. and Podoleanu, A. "A comparative study of noise in supercontinuum light sources for ultra-high resolution optical coherence tomography", Proc. SPIE 10056, Design and Quality for Biomedical Technologies X, 100560O (14 March 2017); https://doi.org/10.1117/12.2251500